THE JOURNAL OF BIOLOGICAL CHEMISTRY
Vol. 278, No. 13, Issue of March 28, pp. 10973–10982, 2003

Printed in U.S.A.

Blue Light Perception in Plants

DETECTION AND CHARACTERIZATION OF A LIGHT-INDUCED NEUTRAL FLAVIN RADICAL IN A C450A MUTANT OF PHOTOTROPIN*

Received for publication, June 4, 2002, and in revised form, December 26, 2002
Published, JBC Papers in Press, January 13, 2003, DOI 10.1074/jbc.M205509200

Christopher W. M. Kay‡, Erik Schleicher‡§, Andreas Kuppig‡, Heidi Hofner§, Wolfhart Rüdiger¶, Michael Schleicher‖, Markus Fischer§, Adelbert Bacher§, Stefan Weber‡, and Gerald Richter§‡‡**

From the ‡Institut für Experimentalphysik, Freie Universität Berlin, Arnimallee 14, 14195 Berlin, Germany, §Lehrstuhl Organische Chemie und Biochemie, Technische Universität München, Lichtenbergstrasse 4, 85747 Garching, Germany, ¶Institut für Botanik, Ludwig-Maximilians-Universität München, Menzinger Strasse 64, 80638 München, Germany, and ‖Institut für Zellbiologie, Ludwig-Maximilians-Universität München, Schillerstrasse 42, 80336 München, Germany

The LOV2 domain of *Avena sativa* phototropin and its C450A mutant were expressed as recombinant fusion proteins and were examined by optical spectroscopy, electron paramagnetic resonance, and electron-nuclear double resonance. Upon irradiation (420–480 nm), the LOV2 C450A mutant protein gave an optical absorption spectrum characteristic of a flavin radical even in the absence of exogenous electron donors, thus demonstrating that the flavin mononucleotide (FMN) cofactor in its photogenerated triplet state is a potent oxidant for redox-active amino acid residues within the LOV2 domain. The FMN radical in the LOV2 C450A mutant is N(5)-protonated, suggesting that the local pH close to the FMN is acidic enough so that the cysteine residue in the wild-type protein is likely to be also protonated. An electron paramagnetic resonance analysis of the photogenerated FMN radical gave information on the geometrical and electronic structure and the environment of the FMN cofactor. The experimentally determined hyperfine couplings of the FMN radical point to a highly restricted delocalization of the unpaired electron spin in the isoalloxazine moiety. In the light of these results a possible radical-pair mechanism for the formation of the FMN-C(4a)–cysteinyl adduct in LOV domains is discussed.

Numerous phenomena in the life cycle of plants such as circadian timing, regulation of gene expression, and phototropism (the adaptive process whereby plants bend toward a light source to maximize light capture for photosynthesis) are responses to ambient light levels in the UV-A and blue spectral regions comprising wavelengths of about 320–500 nm (1–3). Currently, two classes of blue light photoreceptors have been identified in plants; they are the cryptochromes (4–6) and the phototropins (7, 8), both of which are flavoproteins. Phototropins, the blue light photoreceptors for phototropic bending (9, 10), chloroplast relocation (11–13), and stomatal opening (14), have been identified in several plant species including *Arabidopsis thaliana*, *Avena sativa* (oat), *Oryza sativa* (rice), and *Zea mays* (corn) (8). Phototropin of *A. sativa* is a protein comprising 923 amino acids, which is specified by the *phot1* gene (previously designated *nph-1*) (1, 9). The protein contains two 12-kDa flavin mononucleotide (FMN) binding domains. The FMN binding modules belong to the PAS (PER/ARNT/SIM) domain superfamily (15, 16) occurring in many regulatory proteins and have been designated as LOV[1] domains; the acronym is based on the involvement in the signaling of light, oxygen, or voltage levels (10, 17). Very recently, the presence of a LOV domain with similarity to the photoactive LOV domains of the phototropin of higher plants has been identified in the non-photosynthetic soil bacterium *Bacillus subtilis* (18).

After illumination by blue light, recombinant LOV domains of phototropin undergo a transient and fully reversible bleaching of their optical absorption at 400–500 nm accompanied by an increase of absorption at 390 nm (19, 20). Based on the similarity of the spectral characteristics of the photoproduct 19 and that of a kinetically competent intermediate in mercuric ion reductase (21), Vincent Massey[2] suggested that the LOV photocycle comprises a light-induced addition of a thiol group (cysteine 450 of phototropin in the case of the LOV2 domain from *A. sativa*) to the C(4a) position of the flavin chromophore followed by the spontaneous fragmentation of the adduct in the dark (see Fig. 1). This hypothesis could later be confirmed by ^{13}C NMR spectroscopy (22).

Recently, the crystal structure of the LOV2 domain of the phytochrome/phototropin chimeric photoreceptor phy3 from the fern *Adiantum capillus-veneris* was solved at a 2.7 Å resolution (23). The single LOV2 cysteine residue is located 4.2 Å from the flavin atom C(4a). Until now, however, the details of the mechanism of adduct formation have not been conclusively established. The ground state, an intermediate state resembling the FMN triplet (^{3}FMN), and the adduct (19, 20) have been observed in phototropin by optical spectroscopy, whereas with ^{13}C and ^{31}P NMR (22) and x-ray crystallography (24) the ground state and the adduct could be characterized.

Swartz *et al.* (20) propose an ionic reaction pathway for

* This work was supported by VolkswagenStiftung Grant I/77100 (to S. W.) and by the Deutsche Forschungsgemeinschaft, the Fonds der Chemischen Industrie, and the Hans-Fischer-Gesellschaft. The costs of publication of this article were defrayed in part by the payment of page charges. This article must therefore be hereby marked "*advertisement*" in accordance with 18 U.S.C. Section 1734 solely to indicate this fact.

The nucleotide sequence(s) reported in this paper has been submitted to the GenBank™/EBI Data Bank with accession number(s) AF544403.

This paper is dedicated to the memory of Vincent Massey.

** To whom correspondence may be addressed. Tel.: 49-30-838-56139; Fax: 49-30-838-56046; E-mail: Stefan.Weber@physik.fu-berlin.de.

‡‡ To whom correspondence may be addressed. Tel.: 49-89-289-13336; Fax: 49-89-289-13363; E-mail: Gerald.Richter@ch.tum.de.

[1] The abbreviations used are: LOV, light, oxygen, and voltage levels; EPR, electron magnetic resonance; ENDOR, electron-nuclear double resonance; cw, continuous-wave; mw, microwave; hfc, hyperfine coupling; mT, millitesla.

[2] A contribution to discussion at the 13th International Congress on Flavinsand Flavoproteins, August 29–September 4, 1999, Konstanz, Germany.

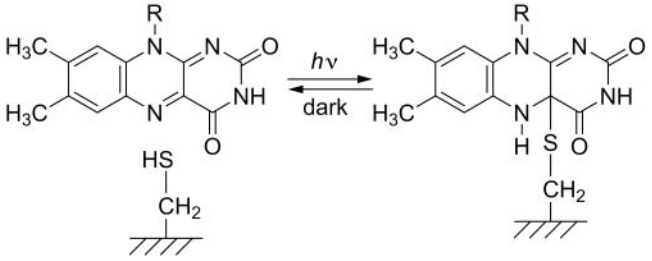

FIG. 1. **The formation of a cysteinyl-flavin-C(4a) covalent adduct in LOV2 after the absorption of blue light by the FMN cofactor.**

FMN-C(4a)–thiol adduct formation with the Cys-450 residue initially present as a thiolate, thus requiring a proton donor other than Cys-450 to protonate the light-generated FMN triplet (20). Recently, however, it has been shown by Fourier transform infrared spectroscopy that the cysteine residue in LOV2 is protonated in the ground state (25), implying that an ionic mechanism, which relies on the presence of a thiolate, is flawed. Thus other potential reaction pathways including a concerted mechanism and a radical-pair mechanism have to be considered. We have therefore investigated both the wild-type *A. sativa* LOV2 domain and a C450A mutant by electron paramagnetic resonance (EPR) spectroscopy. The formation of the FMN-thiol adduct is not possible in the C450A mutant due to the absence of a thiol group. In this case, as will be shown, ^{3}FMN undergoes a photoreduction resembling that observed in photolyases (26–28) and other flavoenzymes with the possible participation of a redox-active amino acid residue, resulting in the formation of a neutral flavin radical, FMNH$^\bullet$. The implications of the observation of FMNH$^\bullet$ are discussed in terms of a possible radical-pair mechanism for adduct formation in LOV domains. The characterization of FMNH$^\bullet$ by EPR and electron-nuclear double resonance (ENDOR) spectroscopy (29) allowed us to probe the geometrical and electronic structure and the environment of the flavin cofactor in the LOV2 domain using the paramagnetic state as a natural spin label.

EXPERIMENTAL PROCEDURES

Construction of an Expression Vector—The open reading frame specifying hisactophilin of *Dictyostelium discoideum* was amplified using the oligonucleotides described in Table I as primers and plasmid pIMS5/c516 as template. The amplified DNA fragment was digested with *Eco*RI and *Hin*dIII and ligated into a pNCO vector (30) that had been treated with the same restriction enzymes. The resulting plasmid pNCO-HISACT-BNH was transformed into *Escherichia coli* strain XL1-Blue.

Construction of Expression Plasmids—The gene segment specifying the *A. sativa* LOV2 domain was excised from the plasmid pCAL-LOV2 (19) by restriction with *Bam*HI and *Hin*dIII. The fragment was ligated into the vector pNCO-HISACT-BNH, which had been treated with the same enzymes. The resulting plasmid designated pNCO-HISLOVWT specifies a fusion protein comprising the LOV2 domain of *phot1* of *A. sativa* and hisactophilin from *D. discoideum* (Fig. 2). An expression plasmid specifying the corresponding C450A mutant was obtained by the same approach starting from the plasmid pCAL-LOV2C450A (19). The plasmids were electro-transformed into *E. coli* strain M15[pREP4].

Protein Expression and Purification—Bacterial cells were grown in LB medium supplemented with ampicillin (180 mg/liter) and kanamycin (15 mg/liter) to an optical density of 0.6 at 600 nm. Isopropyl-thio-β-D-galactopyranoside was added to a final concentration of 1 mM. The cultures were incubated for 5 h, harvested by centrifugation, and stored at −20 °C. Frozen cell mass (5 g) was thawed in 15 ml of buffer A (50 mM Tris hydrochloride, pH 8.0, containing 100 mM NaCl and 2 mM $CaCl_2$) supplemented with 20 mg of lysozyme. The suspension was sonicated and centrifuged. The supernatant was applied to a column of Chelating Sepharose Fast Flow (column volume, 15 ml; Amersham Biosciences), which had been equilibrated with buffer B (50 mM sodium phosphate, pH 8.0, containing 300 mM NaCl) supplemented with 10 mM imidazole. The column was washed with 150 ml of buffer B and was then developed with a linear gradient of 10–500 mM imidazole in buffer B (total volume, 100 ml). Yellow fluorescent fractions were combined and concentrated by ultrafiltration (10-kDa membrane, Pall Gelman, Ann Arbor, MI). The solution was applied to a column of Superdex S75-prep grade (2.6 × 60 cm, Amersham Biosciences), which was developed with 50 mM potassium phosphate, pH 7.5. Yellow fluorescent fractions were combined and concentrated by ultrafiltration to a final concentration of 1 mM as determined photometrically (ϵ_{447} = 13,800 $M^{-1}cm^{-1}$ (19)).

Cleavage of the LOV2 Cys-450 Hisactophilin Fusion Protein by Thrombin—10 mg of LOV2 C450A hisactophilin fusion protein in buffer B supplemented with 2.5 mM $CaCl_2$ were mixed with 50 units of thrombin (Sigma) and incubated overnight at room temperature. The protein solution was applied to a column of Chelating-Sepharose Fast Flow (column volume, 15 ml) that had been equilibrated with buffer B supplemented with 10 mM imidazole. Cleaved LOV2 C450A protein was collected in the flow-through, whereas hisactophilin protein and uncleaved fusion protein remained bound to the column. Yellow fluorescent fractions were combined and concentrated by ultrafiltration through microconcentrators (1-kDa membrane, Pall Gelman, Ann Arbor, MI). Protein homogeneity was monitored by SDS-PAGE electrophoresis.

UV/Visible Measurements—Protein samples (concentration ~0.05 mM) were transferred into an optical cuvette (path length, 1 mm; Hellma, Müllheim, Germany) and supplemented with 0.5 mM EDTA depending on the sample and/or deoxygenated and then illuminated for up to 40 min with 420–480-nm light from a filtered Xe lamp (ILC, PS800SW-1) at room temperature. Decay of the radical was measured in a Shimadzu UV-1601PC (Shimadzu Scientific Instruments, Columbia, MD) spectrophotometer.

Buffer Exchange—Samples were transferred into the desired buffer (usually 70 mM sodium/potassium phosphate, pH 7.0) in H_2O or D_2O by dilution and ultrafiltration through C10 microconcentrators at 4 °C. The cycle was repeated 5 times to give a final D_2O enrichment of 93–97%.

EPR Sample Preparation—The enzyme preparations were transferred into EPR quartz tubes (3-mm inner diameter for X-band (9–10 GHz) EPR; 0.6-mm inner diameter for W-band (95 GHz) EPR) under an argon inert gas atmosphere. They were then illuminated with light of 420–480 nm from a filtered Xe lamp and frozen rapidly in liquid nitrogen.

EPR Instrumentation—Continuous-wave (cw) EPR spectra at X-band frequencies (9–10 GHz) were obtained using a laboratory-built spectrometer. It consists of a Bruker ER041MR microwave (mw) bridge (Bruker, Rheinstetten, Germany) and an AEG-20 electromagnet. Samples were placed in a Bruker ER4118X-MS-5W1 dielectric resonator, which was immersed in a laboratory-built helium gas flow cryostat controlled by a LakeShore 321 temperature controller.

W-band cw-EPR spectra were recorded with a laboratory-built high field EPR spectrometer operating at 94–96 GHz and equipped with a cylindrical TE_{011} cavity. The six-line EPR signal of a Mn(II)/MgO standard, placed near the sample in the cavity, was recorded simultaneously for *g*-factor calibration.

ENDOR Instrumentation—X-band cw-ENDOR spectra were recorded using a laboratory-built spectrometer consisting of an AEG-20 electromagnet and a Bruker ER041MR mw bridge. A radio frequency synthesizer (Hewlett Packard 8647A) in conjunction with a high power radio frequency amplifier (ENI A-300) was used to generate the cw radio frequency field in the laboratory-built TM_{110} ENDOR resonator ($Q \approx 1800$, 1 turn/mm of NMR coil). The temperature was adjusted using a nitrogen-gas flow controlled by a Bruker ER4111VT temperature controller.

Calculations—To assist in the assignment of experimentally determined hyperfine couplings (hfcs) to individual nuclei in the 7,8-dimethyl isoalloxazine moiety of FMNH$^\bullet$, density-functional theory calculations were performed with lumiflavin (7,8,10-trimethyl isoalloxazine) using the program package Gaussian 98 (31). Lumiflavin is considered as a valid model because the ribityl side chain has no significant influence on the electronic structure of FMNH$^\bullet$, which is bound in an extended conformation in the LOV domain. The geometry of the FMNH$^\bullet$ state was optimized at the unrestricted B3LYP/EPR-II level of theory, and single-point calculations of hfcs and electron densities were performed at the same level.

RESULTS

Optical Spectroscopy—Expression vectors specifying fusion proteins comprising the *A. sativa* LOV2 domain (amino acid residues 412–516) or its C450A mutant and the actin binding

TABLE I
Microorganisms, plasmids, and primers used

E. coli strain/plasmid	Relevant characteristics	Reference
M15(pREP4)	lac,ara,gal,mtl,recA$^+$,uvr[pREP4,lacl,kan^r]	60
XL1-Blue	recAI,endAI,gyrA96,thi-1,hsdR17,supE44,rclAl,lac[F′,proAB,lacl^q,lacZΔM15,Tn10(tet^r)]	61
pNCO113	Expression vector for *E. coli*	30, 62
pNCO-HISACT-BNH[a]	pNCO113 with the gene coding for hisactophilin from *D. discoideum*	This study
pNCO-HISLOVWT	pNCO-HISACT-BNH with the gene coding for LOV2 domain of phototropin from *A. sativa*	This study
pNCO-HISLOVC450A	pNCO-HISACT-BNH with the gene coding for LOV2C450A mutant domain of phototropin from *A. sativa*	This study
p1MS5/c516	pUC19 with the gene coding for hisactophilin from *D. discoideum*	63

	Primers for the amplification of the hisactophilin gene (5′–3′)	Restriction site
DD-Hac-Rbs-*Eco*RI-Vo	ATAATAGAATTCATTAAAGAGGAGAAATTAACCATGGGTAACAGAGCATTCAAATCACATC	*Eco*RI
DD-Hac-*Not*I-*Hin*dIII-Hi	TATTATTATAAGCTTAGGAACCAGACGATGCGGCCGCGGATCCAATAATAATTTCTTCAAAGGTGGTG	*Hin*dIII

[a] The nucleotide sequence has been deposited in the GenBank™ database under GenBank™ accession number AF544403.

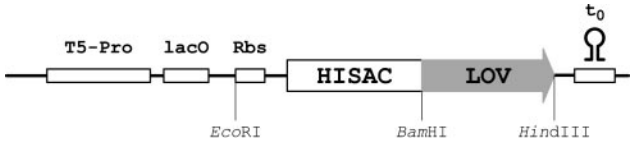

FIG. 2. **Restriction map of the expression cassette of plasmid pNCO-HISLOVWT.** Selected restriction sites are indicated. *T5-Pro*, T5 promoter; *lacO*, lac operator; *Rbs*, ribosome-binding site; t_0, terminator sequence. The schematic is not drawn to scale.

hisactophilin protein from *D. discoideum* were constructed as described under "Experimental Procedures." *E. coli* strains harboring one of these plasmids formed copious amounts of the recombinant fusion protein (about 15% of soluble cell protein), which could be purified easily by affinity chromatography using a nickel-chelate column. The fusion proteins bind tightly to the chelating-Sepharose matrix as a consequence of the abundant histidine residues at the surface of hisactophilin. LOV2 C450A domain, from which the hisactophilin module was cleaved, was prepared with a yield of ~80% as described under "Experimental Procedures." LOV2 C450A domain fused with calmodulin-binding protein was expressed and purified according to published procedures (19).

The optical absorption spectra of the LOV2 C450A domains from the samples under investigation before illumination and after irradiation with blue light ($420 < \lambda < 480$ nm) are shown in Fig. 3. Both fusion proteins have virtually the same ground-state absorbance properties (Fig. 3, *B* and *C*, *solid lines*) as LOV2 protein cleaved from hisactophilin (Fig. 3*A*, *solid line*) but show enhanced stability and solubility. All three proteins have absorption maxima at 363 and 447 nm, characteristic of an FMN chromophore in the oxidized redox state. Shoulders at 425 and 474 nm are vibrational contributions that are well resolved. This is indicative of tight binding between the non-covalently bound FMN and the highly ordered protein structure as well as of the nonpolar nature of the flavin binding pocket.

After continuous blue light irradiation all three LOV2 C450A proteins show the formation of a flavin radical characterized by absorption maxima at 570 and 605 nm (Fig. 3, *dashed* and *dotted lines*). Radical formation occurs in the absence (Fig. 3, *A–C*) and in the presence of an exogenous electron donor such as EDTA (Fig. 3*D*). Furthermore, the radical formation could be observed either in the presence (Fig. 3, *dotted lines*) or in the absence (Fig. 3, *dashed lines*) of oxygen. However, inspection of Fig. 3 clearly shows that the yield of flavin radical differs depending on the protein construct and on the photoreduction conditions. By comparison with the absorption spectra of other flavin radicals in a protein matrix (see, *e.g.* Ref. 27), we conclude that in the fusion protein comprising the LOV2 C450A domain and hisactophilin, supplemented with a 10-fold excess

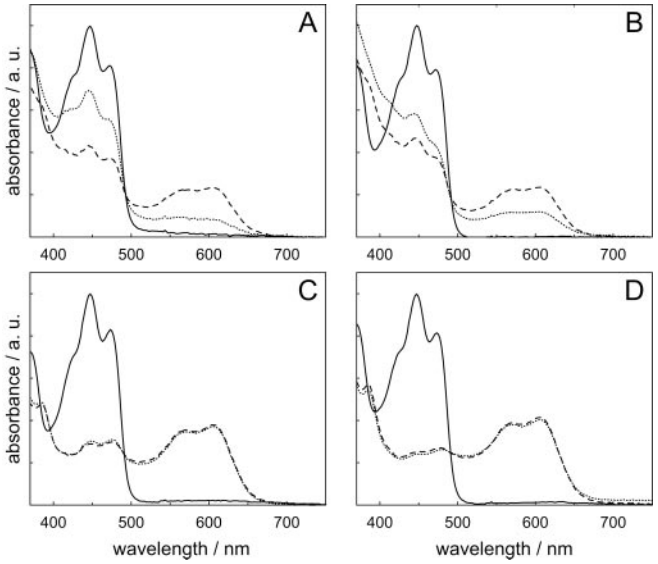

FIG. 3. Normalized optical absorption spectra of FMN bound in *A. sativa* LOV2 C450A domain (*A*), a protein construct comprising the *A. sativa* LOV2 C450A domain and calmodulin (*B*), and a protein construct comprising the *A. sativa* LOV2 C450A domain and hisactophilin (*C*). *Panel D* depicts the optical absorption spectra of the same protein construct as shown in *panel C* but supplemented with a 10-fold excess of EDTA. The *solid lines* are the optical absorption spectra before illumination. The *dashed* and *dotted lines* depict spectra recorded after 40 min (*A* and *B*) and 5 min (*C* and *D*) of blue light illumination in the presence (*dotted lines*, *A–D*) and absence (*dashed lines*, *A–D*) of oxygen. Spectra were recorded at 298 K. *a.u.*, absorbance units.

of EDTA, the FMN cofactor is fully converted from the oxidized to the one-electron reduced semiquinone form (Fig. 3*D*, *dashed line*). To compare the amount of flavin semiquinone radical formed in the various other samples, we compare their absorbances at 605 nm normalized to the LOV2 C450A hisactophilin fusion protein sample supplemented with EDTA (Fig. 3*D*, *dotted line*). The salient points of these data are that the presence of oxygen reduces the radical yield, whereas the presence of either EDTA or the protein fusion partner hisactophilin enhances the radical yield and reduces the oxygen dependence (see Table II).

In all samples investigated, the flavin radical is completely reoxidized in the dark to regenerate oxidized FMN on a time scale of minutes depending on the protein construct and buffer conditions (see Table II). We have monitored this process by observing the absorbance changes at 605 nm as a function of time after blue light illumination (see Fig. 4). Under anaerobic conditions (*squares*) the flavin radical in the cleaved LOV2 C450A domain (Fig. 4*A*) slowly decays with a 1/*e* time constant of (78 ± 7) min, whereas under aerobic conditions (*circles*) the

TABLE II
Decay of the light-induced flavin radical in various A. sativa LOV2 C450A constructs

ND, not determined.

Protein sample	Condition	Radical yield[a]/%	Radical decay[b]/min
LOV2 C450A-hisactophilin	Aerobic	90	8 ± 2
	Anaerobic	92	43 ± 5
	Aerobic + EDTA	97	28 ± 4
	Anaerobic + EDTA	100	31 ± 4
LOV2 C450A-calmodulin-binding protein	Aerobic	29	ND
	Anaerobic	57	ND
LOV2 C450A	Aerobic	20	7 ± 1
	Anaerobic	56	78 ± 7
	Aerobic + EDTA	ND	71 ± 3
	Anaerobic + EDTA	ND	72 ± 3

[a] Typical error; ±5%.
[b] 1/*e* time constants.

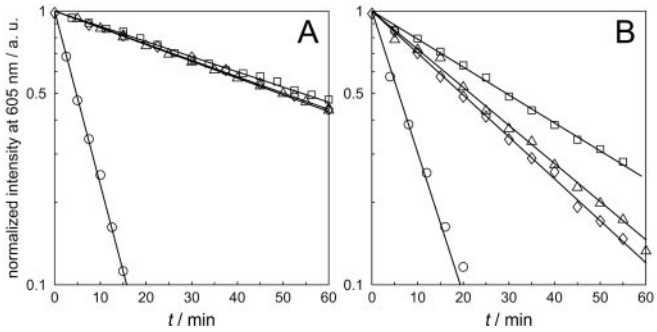

FIG. 4. **Normalized decay of the FMNH· absorption at 605 nm after blue light illumination of the *A. sativa* LOV2 C450A domain (*A*) and a protein construct comprising the *A. sativa* LOV2 C450A domain and hisactophilin (*B*) in the presence (*circles*) and absence (*squares*) of oxygen.** *Triangles* and *diamonds* represent the normalized FMNH· decay curves of the respective samples supplemented with a 10-fold excess of EDTA in the presence (*triangles*) and absence (*diamonds*) of oxygen. Decay curves were recorded at 298 K. The *solid lines* are calculated decays obtained from a least squares fitting of the experimentally determined data points to a monoexponential decay model. *a.u.*, absorbance units.

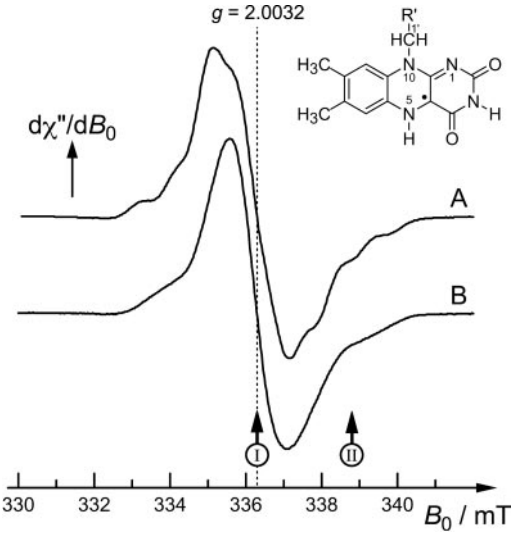

FIG. 5. **X-band frozen solution cw-EPR spectra of FMNH· bound in *A. sativa* LOV2 (C450A mutant) in H_2O (*A*) and D_2O solution (*B*).** The spectra were recorded at 150 K and a mw frequency of 9.4289 GHz, mw power 8 microwatts, and magnetic field modulation amplitude 0.1 mT (100 kHz field modulation). The *arrows* indicate positions at which the ENDOR spectra in Fig. 6 were recorded. *I* is on-center, and *II* is off-center resonance.

radical decay is much faster (7 ± 1 min). In the presence of excess EDTA, the decay times in the absence (*triangles*) or presence (*diamonds*) of oxygen are virtually identical (see Table II).

For the fusion protein comprising the LOV2 C450A domain and hisactophilin, similar trends are observed (Fig. 4*B*). Under anaerobic conditions (*squares*) the flavin radical decays with a 1/*e* time constant of (43 ± 5) min, which is somewhat shorter than that observed for the cleaved LOV2 C450A domain. Under aerobic conditions (*circles*) the radical decays with a 1/*e* time constant of only (8 ± 2) min, which is very close to the value observed for the cleaved LOV2 C450A. In the presence of excess EDTA, the decay times are extended depending on the absence (31 ± 4 min, *triangles*) or presence (28 ± 4 min, *diamonds*) of oxygen.

EPR Spectroscopy—To characterize in more detail the light-induced FMN radical in LOV2 C450A domains, EPR experiments were performed with a sample that was frozen in liquid nitrogen immediately after blue light irradiation. The X-band cw-EPR signal (Fig. 5) reveals a radical signature centered at $g = 2.0032 \pm 0.0001$, which is characteristic for a neutral flavin radical (32, 33). Neutral flavin radicals protonated at N(5) can be distinguished from anion flavin radicals by means of their characteristic peak-to-peak EPR line widths of ≈2.0 and ≈1.5 mT, respectively, which is due to the presence or absence of the large hfc of the proton at N(5) (29, 34). The observed peak-to-peak line width of 2.00 ± 0.01 mT is typical of a neutral flavin radical, FMNH·. The overall line width and line shape of the signal is attributed to the mostly unresolved contributions of hfcs of the unpaired electron spin with ^1H and ^{14}N nuclei of the isoalloxazine moiety of FMN as well as of the protein environment.

To try to detect the EPR signal of a possible second radical species that ought to be created upon electron transfer to FMN in the LOV2 C450A mutant protein, EPR experiments at higher microwave frequencies (95 GHz) and correspondingly larger magnetic fields were also performed (Fig. 6), because overlapping signal contributions from organic radicals are better separated in high magnetic fields due to their differences in *g*-factor.

Even at 95 GHz, only the spectrum arising from one radical species was observed. Scanning over a wider magnetic field range did not reveal any additional signals except for the hyperfine lines of the Mn(II)/MgO standard used for *g*-factor calibration. The signal shown in Fig. 6*A* resembles the frozen-solution spectrum of a neutral flavin radical and is similar to the flavin adenine dinucleotide semiquinone radical observed in DNA photolyase (32). From spectral simulation of the rhombic symmetry of the signal, the principal values of the *g*-matrix, $g_X = 2.0042 \pm 0.0001$, $g_Y = 2.0035 \pm 0.0001$, and $g_Z = 2.0020 \pm 0.0001$ (*X*, *Y*, and *Z* are the principal axes of the *g*-tensor) may be extracted.

Some hyperfine structure emerges in both W-band and X-band EPR spectra (Figs. 5*A* and 6*A*). Although not fully re-

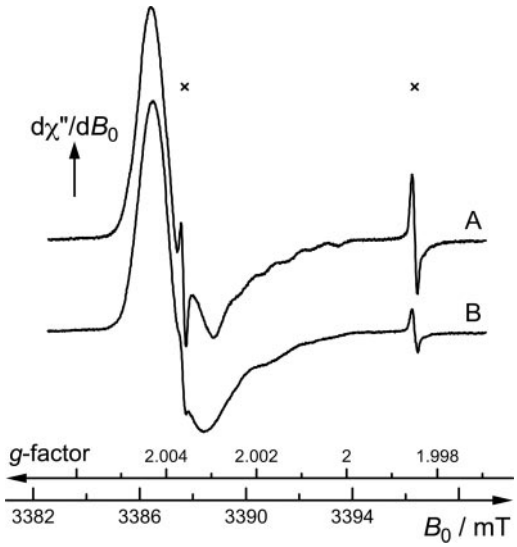

FIG. 6. **W-band frozen solution cw-EPR spectra of FMNH· bound in *A. sativa* LOV2 (C450A mutant) in H_2O (*A*) and D_2O (*B*) solution.** The spectra were recorded at 180 K and a microwave frequency 95.0 GHz, mw power 50 microwatts, and magnetic field modulation amplitude 0.1 mT (8-kHz field modulation). The EPR lines belonging to the Mn(II)/MgO standard used for *g*-factor calibration are indicated with ×'s.

solved, a spacing of 1.05 mT (29 ± 3 MHz) between adjacent shoulders in the signals could be determined. After the procedure outlined previously (32), this hyperfine splitting has been assigned to the hfc tensor component A_z of H (5) (x, y, and z are the principal axes of the H (5) hyperfine tensor based on the following findings. (*a*) The splitting disappears when H (5) is replaced with a deuteron in an exchange of the protonated for deuterated buffer (Figs. 5*B* and 6*B*); (*b*) in the high field EPR experiment, the center of the hyperfine structure shifts toward resonance field values where molecules with their g_z axis aligned parallel to the external magnetic field are in resonance (Fig. 6*A*), which is characteristic for an α-proton; and (*c*) the exchangeable α-proton at N (3) is expected to contribute only marginally to the overall EPR line width due to its small hfc in the 1–2-MHz range (35).

ENDOR Spectroscopy—To characterize in greater detail the electronic structure of the FMN radical, we have also performed ENDOR experiments. For doublet-state radicals, two ENDOR lines are expected per proton hfc tensor component, *A*. When $A < 2\ \nu_H$, the resonance frequencies are

$$\nu_{\mathrm{ENDOR}} = |\nu_H \pm \frac{A}{2}|, \qquad \text{(Eq. 1)}$$

or, when $A > 2\ \nu_H$, the resonance frequencies are

$$\nu_{\mathrm{ENDOR}} = |\frac{A}{2} \pm \nu_H|, \qquad \text{(Eq. 2)}$$

where $\nu_H = g_H\,\mu_H\,B_0/h$ is the proton Larmor frequency at the magnetic field B_0, and μ_H and g_H are the Bohr magneton of a proton and its *g*-value, respectively.

In Fig. 7, *A* and *B*, the X-band cw-ENDOR spectra of the FMN radical cofactor in protonated and deuterated buffer are shown, recorded at a magnetic field of 333.86 mT, corresponding to $g_{\mathrm{iso}} = 2.0032$. The frozen samples give rise to powder-type spectra that are symmetrically centered at the proton Larmor frequency, ν_H.

A group of overlapping signals with hfcs $A \leq 2.0$ MHz forms the so-called "matrix" ENDOR line and is the sum of contributions from the weakly coupled protons at C(7α) and C(9) of the isoalloxazine moiety as well as protons of solvent water and

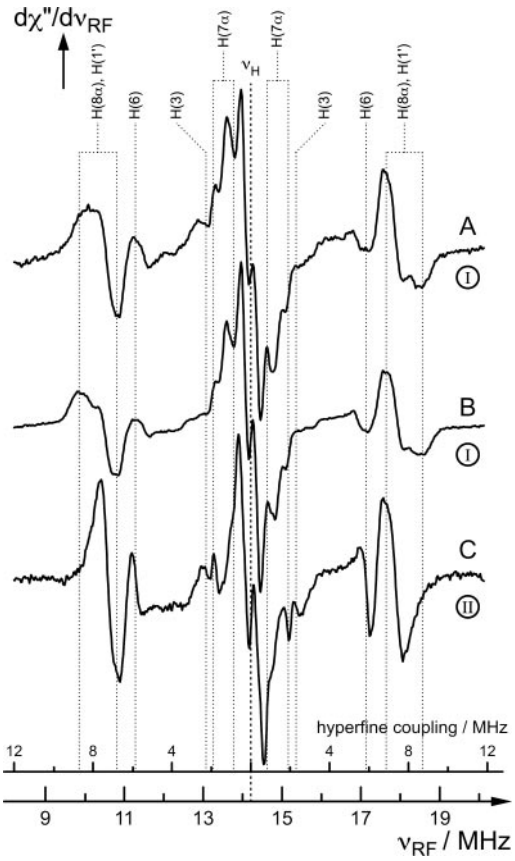

FIG. 7. X-band frozen solution cw-ENDOR spectra of FMNH· bound in *A. sativa* LOV2 (C450A mutant) in H_2O (*A*) and D_2O (*B*) buffer. The spectra were recorded at 150 K with mw power of 4.0 milliwatts, mw frequency of 9.3605 GHz, magnetic field of 333.86 mT (on-center resonance, see the *arrow I* in Fig. 5), and radio frequency modulation amplitude of 40 kHz (19-kHz frequency modulation). *C*, X-band frozen solution cw-ENDOR spectrum in deuterated buffer recorded at 336.36 mT (off-center resonance, see *arrow II* in Fig. 5). υ_{RE}, radio frequency.

amino acid residues near the cofactor-binding site. Their individual signal contributions are not readily assigned. One conclusion, however, may be drawn from a comparison of the matrix lines of the protein in protonated and deuterated buffer (Fig. 7, *A* and *B*); the remarkably small differences in intensity and shape indicate that the cofactor-binding site comprises mostly non-exchangeable protons.

A pair of lines with an hfc of 2.3 ± 0.1 MHz is located next to the matrix region (Fig. 7*A*). Based on the disappearance of these signals upon buffer deuteration (Fig. 7*B*) they are assigned to the proton at N(3), see Table III.

When comparing the protonated and deuterated samples in the region where the resonances of H(6) and the methyl protons H(8α) are expected, two changes become obvious. First, there is a feature at 10.2 MHz that does not appear at 18.2 MHz in the protonated sample (Fig. 7*A*). At first glance this might be due to a large nitrogen hfc tensor. Upon deuteration, however, the spectrum is restored to symmetry, demonstrating that this feature is due to a proton hfc tensor component (Fig. 7*B*). It must be a very large hfc tensor component that has been reflected through zero frequency, because it only appears on one side of ν_H. From Equation 2, a hfc of 48.8 ± 1 MHz may be estimated. This can only be the A_y component of H (5). There should be a partner transition at 38.6 MHz, but it has not been detected. Second, the features at 10.7 and 17.7 MHz decrease in intensity on going from protonated to deuterated buffer. This indicates that another hfc component, again from an exchangeable proton, has resonances at these frequencies. This hfc com-

TABLE III
Experimental hyperfine couplings of FMNH· protons in the C450A Mutant of A. sativa LOV2

Signs of hyperfine couplings have not been determined experimentally but given in comparison with density-functional theory calculations (35).

Atom position	$A_\perp$/MHz	$A_\parallel$/MHz	A_{iso}/MHz
H(3)[a]			−2.3
H(5)[b]			−29
H(6)[a]			−5.9
H(7α)[a]	−1.9	−0.9	−1.6
H(8α)[a]	6.8	8.7	7.4

[a] All hyperfine couplings are accurate within ±0.1 MHz except for the $A_\perp$ and $A_\parallel$ components of H(8α) for which the errors are ±0.1 and ±0.2 MHz, respectively.
[b] From EPR spectra (error ± 3 MHz).

ponent of 7.0 ± 0.5 MHz is, therefore, assigned to the smallest component, A_x, of H (5). α-Protons in a CH segment of a planar π system are predicted to resonate at $A_x \approx 0.5 \times A_{iso}$, $A_z \approx A_{iso}$, and $A_y \approx 1.5 \times A_{iso}$ (36). For the H(5) of FMNH· in LOV2 C450A, the anisotropy is even larger, almost approaching 70% of A_{iso}.

The remaining pronounced hfcs are expected to come from the methyl protons at C(8α). Yet the pattern that is observed in the spectrum of the sample in deuterated buffer is still not typical of the axial symmetry expected from a freely rotating methyl group. Rather it is also an overlap of two roughly axial symmetric proton hfc tensors. This is clear from the inflections observed at 10.7 and 17.7 MHz. The only other proton that can have such a large hfc and with the correct axial symmetry is one of the β-protons at C(1′).

Two different hfcs are expected for the two β-protons at position C(1′). The distance of these protons to N(10) (which carries a high spin density) is rather large, and the anisotropic dipolar coupling is, therefore, relatively small. They may have a large Fermi contact hfc interaction, A_{iso}, however, which varies with the twist angle θ between the N(10)s $2p_z$ orbital and the plane defined by the N(10)–C(1′) bond and the respective C(1′)–H bond. A $\cos^2$ dependence of the splitting is expected if the coupling is caused by hyperconjugation (37, 38). From the x-ray structure of the LOV2 domain (23), θ is 4.9°. Taking this angle into account in a model structure of the isoalloxazine ring and the ribityl side chain and calculating hfcs using density-functional theory gives values of 7.4 and 2.6 MHz for A_{iso} of the more strongly and the more weakly coupled proton at C(1′), respectively.

Deconvolution of $A\|$ and $A_\perp$ of the methyl groups at C(7α) and C(8α) and the β-protons at C(1′) is accomplished utilizing orientation-selection effects that appear when ENDOR spectra are recorded at off-center magnetic field positions (Fig. 7*C*) in the EPR spectrum, as indicated in Fig. 5. The outer parts of the FMNH· EPR signal predominantly arise from molecules with ^{14}N nuclear quantum number values of either +1 or −1 that have their molecular plane perpendicular to the magnetic field. Hence, by desaturation of the spectral wings of the EPR signal, single-crystal like ENDOR spectra can be expected where only those components of the proton hfc tensors are detected that have their axes parallel to the respective component of the dominating ^{14}N hfc tensors, N(5) and N(10). In the case of methyl protons this is the $A_\perp$ component (perpendicular to the cylindrical axis of the rotating methyl group). Similar selection principles apply for the β-protons at C(1′). From the two ENDOR lines with hfcs of 8.7 and 6.8 MHz, only the latter may be detected at off-center field settings. Therefore, these two signals may be assigned as the $A\| = 8.7 \pm 0.3$ MHz and $A_\perp = 6.8 \pm 0.1$ MHz components of the hfc tensor of H(8α) and the more strongly coupled proton at C(1′), giving $A_{iso} = 7.4 \pm 0.2$ MHz (see Table III).

The off-center field ENDOR experiment has enabled the identification of the hfc due to the methyl group at C(7α) even though the assignment is more difficult due to the small size of this coupling. Nevertheless, a value of 1.6 ± 0.1 MHz for A_{iso} (see Table III) could be obtained for this nucleus in accordance with the following evidence. First, both the $A\|$ and $A_\perp$ features can still be observed after H_2O/D_2O buffer exchange (see Fig. 7, *A* and *B*), demonstrating that the corresponding proton is neither exchangeable nor a true matrix proton. In the orientation-selection experiment (see Fig. 7*C*) only the $A_\perp$ component should be observed. Indeed, in the correct region around 2 MHz, there is a major change upon orientation selection. This feature may, therefore, be assigned to $A\|$.

Finally, the hfc 5.9 ± 0.1 MHz due to H(6) could also be detected and assigned from the orientation-selection ENDOR experiment. This is an α-proton and would be expected to be of rhombic shape. Typically, only the central crossing point in the powder ENDOR spectrum of this hfc tensor is visible. It is usually assigned to A_{iso}, which is a good assumption as long as the tensorial pattern is symmetric around A_{iso}.

DISCUSSION

Blue light irradiation converts the wild-type LOV2 domain into an FMN-C(4a)-cysteinyl adduct via the FMN triplet state. Illumination of the LOV2 C450A mutant with blue light has also been shown to produce a flavin triplet (20), ^{3}FMN; however, the subsequent generation of a flavin radical has not yet been reported. Here we have shown that in the LOV2 C450A mutant, electron transfer to ^{3}FMN takes place, with the participation of an as yet to be identified amino acid residue (*X*′ in Fig. 8), resulting in the formation of a neutral FMN radical, FMNH·.

The observation of FMNH· is independent of protein construct and buffer conditions such as the presence of an exogenous reductant. This is in contrast to the well known photoreduction of flavoproteins (described by Massey and Palmer (39)) in which supplemented electron donors are required for flavin semiquinone generation. Therefore, we conclude that in the LOV2 C450A domains the flavin radical is formed by intraprotein electron transfer from a redox-active amino acid. Tryptophan, histidine, or tyrosine are likely candidates for electron transfer to flavin triplets (due to their lower redox potential compared with that of ^{3}FMN) as has been shown previously by laser flash photolysis (40, 41).

The amount of FMNH· produced is different for the various LOV2 samples, and these variations deserve some comment. In principle, the radical yield reflects the competition between radical formation and its decay, the latter occurring via either back electron transfer or reoxidation of FMNH· by molecular oxygen to form FMN and O_2^- (42). Radical formation is enhanced in the LOV2 C450A hisactophilin construct compared with the cleaved LOV2 C450A domain and the calmodulin-fused protein. This may be understood by the superior electron-donating capabilities of the hisactophilin moiety, which contains 31 histidines and three tyrosines as potentially redox-active amino acid residues (43). Thus, either additional electron transfer pathways are operating or the initial electron hole generated by electron transfer to ^{3}FMN within the LOV2 moiety of the construct further migrates into the hisactophilin domain. In comparison, the cleaved LOV2 domain contains only one histidine, three tyrosines, and one tryptophan as likely candidates for electron donation to the FMN cofactor. The alignment of the LOV2 domains from *A. capillus-veneris* and *A. sativa* shows that these amino acids are conserved (23). In the x-ray structure of *Adiantum* LOV2, they are located at the surface of the domain, at least 11 Å away from the isoallox-

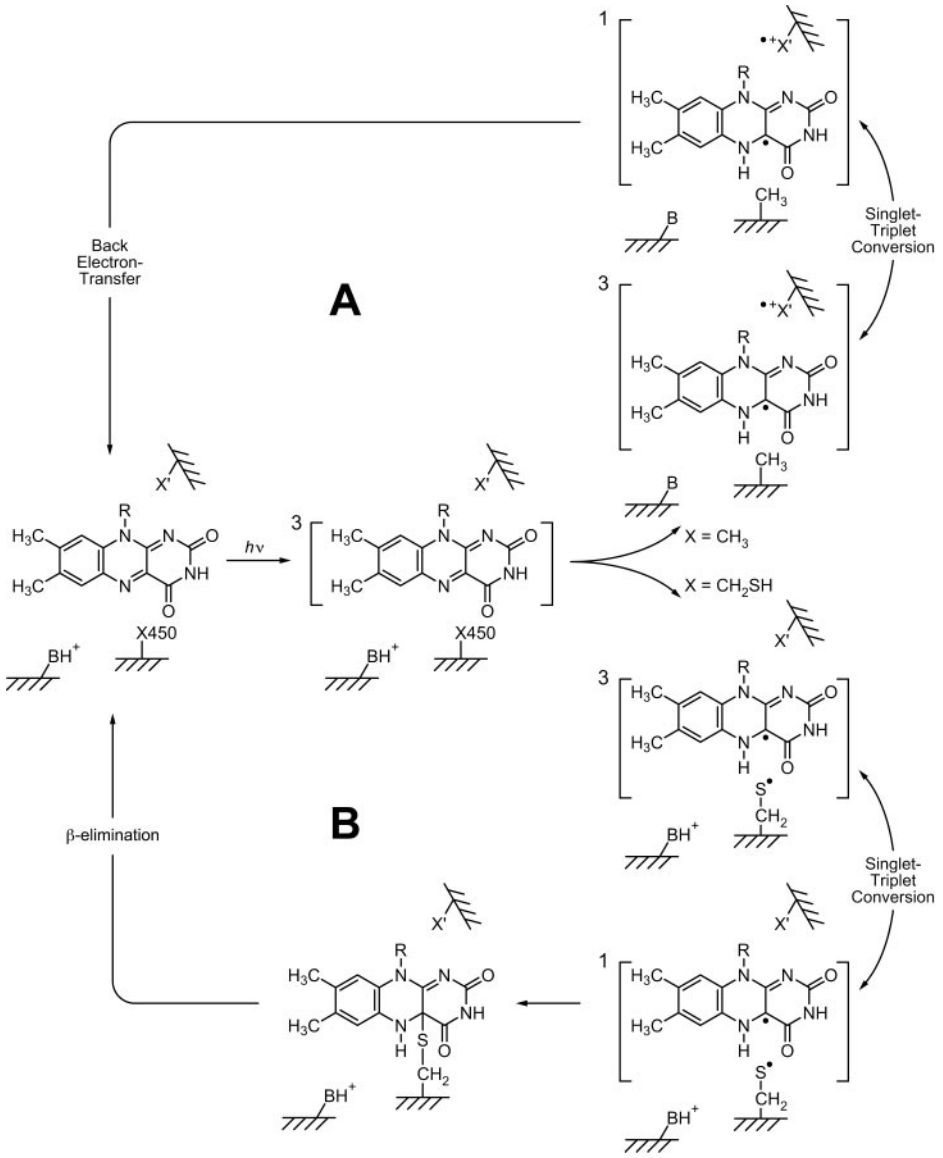

FIG. 8. **Hypothetical radical-pair mechanism for the formation of the FMNH· radical in the LOV2 C450A mutant (*A*) or the FMN-C(4a)–cysteinyl adduct in wild-type LOV2 domains (*B*) after absorption of blue light by the FMN cofactor.** *X′* is an as yet unidentified redox-active amino acid residue in the protein backbone.

azine ring of FMN (23). Although only the FMN radical but not its redox partner has been detected, its observation is nevertheless consistent with an intraprotein electron transfer. We conclude that the redox partner is either degraded or that more than one amino acid may act as an electron donor to FMN.

Reoxidation of FMNH· by molecular oxygen is expected to be similar for all three LOV2 samples, as is indeed observed experimentally (Fig. 4). Under aerobic conditions, this is clearly the preferred process for regeneration of oxidized FMN and, therefore, dominates flavin radical decay kinetics. Under anaerobic conditions, radical decay occurs via back electron transfer to regenerate the thermodynamically more stable oxidized FMN. Again, the hisactophilin-fused LOV2 domain provides more efficient electron transfer pathways compared with the cleaved LOV2 domain, and therefore, radical decay is enhanced in the recombinant fusion protein.

The situation is different in the presence of EDTA. EDTA is a well known reducing agent for photoexcited flavin triplet states (39). In solution studies, triplet flavin abstracts a hydrogen atom from EDTA, forming a neutral flavin radical, whereas the ETDA then decarboxylates and fragments to produce stable products (44, 45). However, in the photoreduction of LOV2 C450A, EDTA has only minor influence on the measured radical yields (Fig. 3, *C* and *D*), which indicates that FMNH· is almost exclusively formed by intraprotein electron transfer rather than by reaction of ^{3}FMN with EDTA. On the other hand, in the presence of EDTA, the reoxidation of FMNH· becomes independent of oxygen content (Fig. 4, *diamonds* and *triangles*). Qualitatively, this finding may be understood in terms of the EDTA sequestering trace amounts of transition metal ions (that are unavoidably present as impurities from the protein preparation) that, if not chelated, may act as catalysts in the activation of molecular oxygen (46, 47). Thus, EDTA plays its well known antioxidant role by preventing reoxidation of the flavin.

Once FMNH· is generated, its decay is extremely slow (Fig. 4). This is even more evident when taking into account the small size of the LOV2 domain (23). Electron transfer time constants in the sub-microsecond range are observed in other flavoproteins; for example, in photolyases in which electrons are transferred over distances exceeding the diameter of LOV domains (28). This demonstrates that, in contrast to many other flavoproteins, low activation energy electron transfer pathways do not exist in the LOV2 domain or that endergonic steps in the electron transfer pathway have to be considered. Nevertheless, both redox forms of the FMN chromophore, oxidized and one-electron reduced, are well stabilized by the protein matrix. Hence, overall the excited-state flavin is optimized

to undergo electron transfer but the electron transfer pathways leading to the surface of the LOV2 domain are inefficient. This may be necessary so that adduct formation with Cys-450 in the wild-type, which takes place on a microsecond time scale (20, 48), could dominate alternative electron transfer processes. From this study we cannot directly draw conclusions about the time scale or quantum yield of the forward electron transfer observed in the LOV2 C450A domain. A slowdown of electron transfer by roughly an order of magnitude is expected for every 2-Å increase of distance between the redox partners, if other parameters such as protein packing density, free energy, and reorganization energy remain comparable (49). Thus, in comparison to a possible electron transfer from Cys-450 (which is 4.2 Å away from C(4a) of FMN) to ^{3}FMN in the wild-type a roughly 10^4-fold decreased rate of electron transfer from one of the other (more distant) redox-active amino acids in the LOV2 domain to ^{3}FMN would be expected. This decrease, however, is predicted to make the electron transfer rate so slow that ^{3}FMN would be mostly converted back to the ground state before electron transfer could happen. Thus, the quantum yield of electron transfer should be rather low. This is most likely the reason why in previous laser-flash photolysis studies no flavin radical formation was observed, whereas by using continuous irradiation in this study, a flavin radical was generated at high yield. Taken together, these observations have several major implications for adduct formation in LOV domains, which will now be considered.

Swartz *et al.* (20) propose an ionic reaction pathway with the Cys-450 residue initially present as a thiolate. In this mechanism, ^{3}FMN is protonated at N(5) by a nearby and as yet unidentified proton-donating group in the protein to give the $FMNH^+$ cation. Upon protonation of N(5) (which occurs in the ground state FMN only at pH $\approx$ 0), the electron density distribution of the isoalloxazine ring is altered due to the nonbonding pair of electrons at N(5) becoming a bonding pair with the additional proton. The $FMNH^+$ carbocation, which formally has a positive charge at C(4a), is the electrophile that can then form a bond with the nucleophilic thiolate, thus generating the adduct. The hypothetical ionic mechanism also requires that Cys-450 is present as a thiolate and simultaneously that ^{3}FMN is protonated before adduct formation occurs. Yet in solution it has been demonstrated that flavin triplet protonation occurs only at pH $<$ 4.4 (50–52). At higher pH, ^{3}FMN undergoes electron transfer followed by protonation when the pH is $<$8.3 to form a neutral flavin radical (50) rather than the anion radical, $FMN^{\bullet-}$. These facts seem to be somewhat contradictory, and although it is not unreasonable that the local pH at the FMN-binding site could be rather low given the proximity of FMN and C450, it seems unlikely that the latter could at the same time be deprotonated (pK_a of cysteine in solution, 8.37). Furthermore, it has recently been shown by Fourier transform infrared spectroscopy that the cysteine residue is protonated in the ground state (25).

An alternative that is consistent with our experimental observations is a radical pair mechanism (see Fig. 8*B*; for review, see Ref. 53). ^{3}FMN is an extremely efficient oxidizing agent in the presence of electron donors such as EDTA or redox-active amino acids in solution (40, 41) and in various proteins, including the LOV2 domain, as demonstrated in this study. A flavin semiquinone is formed from ^{3}FMN in a one-electron photoreduction that may be followed by proton transfer depending on the pH to give the anionic or neutral flavin radical (39).

In the wild-type LOV2 domain ^{3}FMN could abstract an electron from Cys-450 and a spin-correlated ionic radical pair consisting of an anionic flavin radical, $FMN^{\bullet-}$, and a sulfur-centered radical, $RS^{\bullet+}H$, would be formed. This could undergo subsequent proton transfer to give the neutral flavin radical, $FMNH^{\bullet}$, and a sulfur-centered radical, $RS^{\bullet}$. Alternatively, ^{3}FMN could directly abstract a hydrogen atom from cysteine, giving the same product, a neutral radical pair. A radical pair created from a triplet state precursor has initially the same spin state (*i.e.* $^3[FMNH^{\bullet} \cdots RS^{\bullet}]$), due to the conservation of angular momentum, and thus cannot form a covalent bond. At first glance this might be thought to rule out adduct formation via a radical-pair mechanism or that radical pairs should have been detected in the wild type, which has not been the case to date. A covalent bond and, hence, the FMN-cysteinyl adduct may only form if the spin state of the radical pair evolves to obtain a singlet character by singlet-triplet mixing: $^3[FMN^{\bullet} \cdots RS^{\bullet}] \leftrightarrow {}^1[FMN^{\bullet} \cdots RS^{\bullet}]$. Because of strong spin-orbit coupling in sulfur-centered radicals (spin-orbit coupling constant, 382 cm^{-1}), however, a mechanism for extremely rapid singlet-triplet interconversion exists. At room temperature, in solution, these radicals have been shown to have relaxation times in the nanosecond regime (54). Hence, if spin mixing occurs on this time scale or even faster, the covalent adduct will be formed on the same time scale, which implies that the lifetime of the intermediate radical pair will be too short for detection by EPR. That they were not detected by optical methods simply implies that their short-lived absorption may be swamped by the background of relatively long-lived ^{3}FMN and adduct.

The spin chemistry is also important for the hypothetical ionic mechanism discussed by Swartz *et al.* (20) and for a possible concerted mechanism. Given that adduct formation proceeds via ^{3}FMN, then $FMNH^+$ and the adduct must also be created in the triplet state. That the adduct would be created in a triplet state is rather unlikely, but if it were, its spin state would have been evident from its effect on the NMR line widths, yet no line broadening was observed (22). The only possibility is that $FMNH^+$ converts to the singlet ground state before the adduct is formed. This is certainly possible under the influence of the sulfur atom, but the singlet ground state would almost certainly deprotonate before adduct could form (recall that the ground-state flavin is a much weaker base than the excited state (55)).

In a hypothetical radical-pair mechanism these requirements are relaxed. Electron transfer may occur with either a protonated or deprotonated cysteine residue (40, 41). Flavin protonation at N(5) from either the cysteine or another donor group can occur either during the radical-pair lifetime or after the adduct has been formed. An important point is that protonation of ^{3}FMN is not necessarily the rate-determining step in a radical-pair mechanism, whereas it should be in an ionic mechanism.

The minimal differences in the matrix region of the ENDOR spectra in protonated and deuterated buffer are also of interest. Although the x-ray structure does not show the presence of any water molecules close to the FMN isoalloxazine ring, this does not necessarily prove that the cofactor is in a water-free environment. Often in flavoenzymes the matrix region collapses upon buffer deuteration. This is especially true where a substrate approaches the flavin cofactor very closely to facilitate, for example, hydrogen ion transfer (56). In DNA photolyases, the matrix region is slightly altered, and it is known from its x-ray structure (57) that the cofactor is mostly buried in the protein and isolated from solvent water. In the C450A mutant of phototropin, the changes in the ENDOR spectrum are minimal. No exogenous substrate needs to approach the FMN cofactor, because the cysteine is an integral part of the protein. The flavin triplet state is a very reactive species that must be isolated so that it may only perform its biological function; that is, adduct formation. In LOV2 domains, ^{3}FMN is protected

from reacting with (*a*) molecular oxygen with which it may generate either singlet oxygen or a FMN-C(4a)–peroxide adduct (hence, the slow reoxidation of $FMNH^{\bullet}$ to form FMN and $O_2^{\bullet-}$), (*b*) potential exogenous electron donors (hence, the small influence of EDTA on the radical yield), and (*c*) distant redox-active amino acids that may deactivate ^{3}FMN to form a stable FMN radical (hence, the slow forward and backward electron transfer rates in LOV2 C450A).

The proton hfcs also allow some information on the electronic structure of the cofactor to be drawn. First, the A_{iso} hfc from the methyl H(8α) protons determined by ENDOR, which is usually considered a guide to the overall spin-density distribution (due to its ease of determination) is one of the smallest yet determined (32, 58). This further supports the rather isolated situation of the FMN cofactor in the LOV2 domain and points to a rather nonpolar cofactor-binding site (59). Second, A_{iso} for H (5) determined by EPR is substantially larger than that observed in DNA photolyase (32). Taken together, these hfcs indicate that the unpaired electron is, rather, localized toward the pyrimidine ring of the isoalloxazine moiety. A localization of the unpaired electron would be expected to aid the efficient formation of a bond between the flavin radical and the cysteinyl radical in a radical pair mechanism.

CONCLUSIONS

Our work unambiguously shows that the flavin cofactor of the LOV2 domain has electron transfer properties. Hence, in the wild type there must be a competition between adduct formation and the electron transfer reaction with another as yet unidentified amino acid residue. Nevertheless, adduct formation is the overwhelmingly dominant process in wild-type LOV2; no radicals are observed in the wild type that may be irradiated (reversibly) for long periods without suffering degradation (22). Previous optical studies have determined that adduct formation occurs on the microsecond time scale (20, 48). Hence, the competing electron transfer reaction observed in the mutant must be much less efficient and, hence, slower to ensure that only FMN-cysteinyl adduct formation occurs. This is in contrast to other flavoenzymes such as the structurally unrelated photolyases, where the photoreduction from the fully oxidized flavin proceeds on a nanosecond time scale (28). It would be surprising, therefore, if the crucial step in adduct formation were, as previously postulated (20), a proton transfer rather than an electron transfer, given that it should be significantly faster than the alternative electron transfer process observed in the C450A mutant.

The observation of a neutral flavin radical rather than an anion flavin radical gives information on the local pH of the flavin moiety. In aqueous solution, a neutral flavin radical is only formed at pH values < 8.3. Consequently, we conclude, in agreement with a recent Fourier-transform infrared study, that it is likely that the cysteine is at least partially protonated in the wild-type protein.

Although the evidence presented here is consistent with a radical-pair mechanism for adduct formation, it is still not proven. This question has to be addressed by time-resolved EPR and chemically induced dynamic nuclear polarization experiments that are presently being performed in our laboratory.

Acknowledgments—We thank Dr. Michael Salomon and Elke Knieb for generously providing the plasmids pCAL-LOV2 and pCAL-LOV2C450A. We thank Professor Robert Bittl (Free University Berlin) and Professor Maria-Elisabeth Michel-Beyerle (Technical University Munich) for helpful discussions. Continued support by Professor Möbius is gratefully acknowledged.

REFERENCES

1. Short, T. W., and Briggs, W. R. (1994) *Annu. Rev. Plant Physiol. Plant Mol. Biol.* **45,** 143–171
2. Lin, C. (2000) *Trends Plant Sci.* **5,** 337–342
3. Briggs, W. R., and Olney, M. A. (2001) *Plant Physiol.* **125,** 85–88
4. Cashmore, A. R., Jarillo, J. A., Wu, Y.-J., and Liu, D. (1999) *Science* **284,** 760–765
5. Devlin, P. F., and Kay, S. A. (1999) *Trends Cell Biol.* **9,** 295–298
6. Devlin, P. F., and Kay, S. A. (2001) *Annu. Rev. Physiol.* **63,** 677–694
7. Briggs, W. R., and Huala, E. (1999) *Annu. Rev. Cell Dev. Biol.* **15,** 33–62
8. Briggs, W. R., Beck, C. F., Cashmore, A. R., Christie, J. M., Hughes, J., Jarillo, J. A., Kagawa, T., Kanegae, H., Liscum, E., Nagatani, A., Okada, K., Salomon, M., Rüdiger, W., Sakai, T., Takano, M., Wada, M., and Watson, J. C. (2001) *Plant Cell* **13,** 993–997
9. Liscum, E., and Briggs, W. R. (1995) *Plant Cell* **7,** 473–485
10. Huala, E., Oeller, P. W., Liscum, E., Han, I.-S., Larsen, E., and Briggs, W. R. (1997) *Science* **278,** 2120–2123
11. Kagawa, T., Sakai, T., Suetsugu, N., Oikawa, K., Ishiguro, S., Kato, T., Tabata, S., Okada, K., and Wada, M. (2001) *Science* **291,** 2138–2141
12. Jarillo, J. A., Gabrys, H., Capel, J., Alonso, J. M., Ecker, J. R., and Cashmore, A. R. (2001) *Nature* **410,** 952–954
13. Sakai, T., Kagawa, T., Kasahara, M., Swartz, T. E., Christie, J. M., Briggs, W. R., Wada, M., and Okada, K. (2001) *Proc. Natl. Acad. Sci. U. S. A.* **98,** 6969–6974
14. Kinoshita, T., Doi, M., Suetsugu, N., Kagawa, T., Wada, M., and Shimazaki, K.-i. (2001) *Nature* **414,** 656–660
15. Zhulin, I. B., Taylor, B. L., and Dixon, R. (1997) *Trends Biochem. Sci.* **22,** 331–333
16. Taylor, B. L., and Zhulin, I. B. (1999) *Microbiol. Mol. Biol. Rev.* **63,** 479–506
17. Christie, J. M., Salomon, M., Nozue, K., Wada, M., and Briggs, W. R. (1999) *Proc. Natl. Acad. Sci. U. S. A.* **96,** 8779–8783
18. Losi, A., Polverini, E., Quest, B., and Gärtner, W. (2002) *Biophys. J.* **82,** 2627–2634
19. Salomon, M., Christie, J. M., Knieb, E., Lempert, U., and Briggs, W. R. (2000) *Biochemistry* **39,** 9401–9410
20. Swartz, T. E., Corchnoy, S. B., Christie, J. M., Lewis, J. W., Szundi, I., Briggs, W. R., and Bogomolni, R. A. (2001) *J. Biol. Chem.* **276,** 36493–36500
21. Miller, S. M., Massey, V., Ballou, D., Williams, C. H., Distefano, M. D., Moore, M. J., and Walsh, C. T. (1990) *Biochemistry* **29,** 2831–2841
22. Salomon, M., Eisenreich, W., Dürr, H., Schleicher, E., Knieb, E., Massey, V., Rüdiger, W., Müller, F., Bacher, A., and Richter, G. (2001) *Proc. Natl. Acad. Sci. U. S. A.* **98,** 12357–12361
23. Crosson, S., and Moffat, K. (2001) *Proc. Natl. Acad. Sci. U. S. A.* **98,** 2995–3000
24. Crosson, S., and Moffat, K. (2002) *Plant Cell* **14,** 1067–1075
25. Iwata, T., Tokutomi, S., and Kandori, H. (2002) *J. Am. Chem. Soc.* **124,** 11840–11841
26. Heelis, P. F., and Sancar, A. (1986) *Biochemistry* **25,** 8163–8166
27. Gindt, Y. M., Vollenbroek, E., Westphal, K., Sackett, H., Sancar, A., and Babcock, G. T. (1999) *Biochemistry* **38,** 3857–3866
28. Weber, S., Kay, C. W. M., Mögling, H., Möbius, K., Hitomi, K., and Todo, T. (2002) *Proc. Natl. Acad. Sci. U. S. A.* **99,** 1319–1322
29. Edmondson, D. E. (1985) *Biochem. Soc. Trans.* **13,** 593–600
30. Richter, G., Fischer, M., Krieger, C., Eberhardt, S., Lüttgen, H., Gerstenschläger, I., and Bacher, A. (1997) *J. Bacteriol.* **179,** 2022–2028
31. Frisch, M. J., Trucks, G. W., Schlegel, H. B., Scuseria, G. E., Robb, M. A., Cheeseman, J. R., Zakrzewski, V. G., Montgomery, J. A., Stratmann, R. E., Burant, J. C., Dapprich, S., Millam, J. M., Daniels, A. D., Kudin, K. N., Strain, M. C., Farkas, O., Tomasi, J., Barone, V., Cossi, M., Cammi, R., Mennucci, B., Pomelli, C., Adamo, C., Clifford, S., Ochterski, J., Petersson, G. A., Ayala, P. Y., Cui, Q., Morokuma, K., Malick, D. K., Rabuck, A. D., Raghavachari, K., Foresman, J. B., Cioslowski, J., Ortiz, J. V., Stefanov, B. B., Liu, G., Liashenko, A., Piskorz, P., Komaromi, I., Gomperts, R., Martin, R. L., Fox, D. J., Keith, T., Al-Laham, M. A., Peng, C. Y., Nanayakkara, C., Gonzalez, M., Challacombe, M., Gill, P. M. W., Johnson, B. G., Chen, W., Wong, M. W., Andres, J. L., Head-Gordon, M., Replogle, E. S., and Pople, J. A. (1998), *Gaussian 98*, Version A7, Gaussian Inc., Pittsburgh, PA
32. Kay, C. W. M., Feicht, R., Schulz, K., Sadewater, P., Sancar, A., Bacher, A., Möbius, K., Richter, G., and Weber, S. (1999) *Biochemistry* **38,** 16740–16748
33. Fuchs, M., Schleicher, E., Schnegg, A., Kay, C. W. M., Törring, J. T., Bittl, R., Bacher, A., Richter, G., Möbius, K., and Weber, S. (2002) *J. Phys. Chem. B* **106,** 8885–8890
34. Edmondson, D. E., and Tollin, G. (1983) *Top. Curr. Chem.* **108,** 109–138
35. Weber, S., Möbius, K., Richter, G., and Kay, C. W. M. (2001) *J. Am. Chem. Soc.* **123,** 3790–3798
36. Carrington, A., and McLachlan, A. D. (1967) *Introduction to Magnetic Resonance*, pp. 103–107, Harper & Row, New York
37. Heller, C., and McConnell, H. M. (1960) *J. Chem. Phys.* **32,** 1535–1539
38. Horsfield, A., Morton, J. R., and Whiffen, D. H. (1961) *Mol. Phys.* **4,** 425–431
39. Massey, V., and Palmer, G. (1966) *Biochemistry* **5,** 3181–3189
40. Heelis, P. F., Parsons, B. J., and Phillips, G. O. (1979) *Biochim. Biophys. Acta* **587,** 455–462
41. Heelis, P. F., and Phillips, G. O. (1979) *Photobiochem. Photobiophys.* **1,** 63–70
42. Bruice, T. C. (1984) *Isr. J. Chem.* **24,** 54–61
43. Scheel, J., Ziegelbauer, K., Kupke, T., Humbel, B. M., Noegel, A. A., Gerisch, G., and Schleicher, M. (1989) *J. Biol. Chem.* **264,** 2832–2839
44. Traber, R., Kramer, H. E. A., and Hemmerich, P. (1982) *Biochemistry* **21,** 1687–1693
45. Tollin, G. (1995) *J. Bioenerg. Biomembr.* **27,** 303–309
46. Pierre, J. L., and Fontecave, M. (1999) *Biometals* **12,** 195–199
47. Sun, J., and Stanbury, D. M. (2002) *Inorg. Chim. Acta* **336,** 39–45

48. Holzer, W., Penzkofer, A., Fuhrmann, M., and Hegemann, P. (2002) *Photochem. Photobiol.* **75,** 479–487
49. Page, C. C., Moser, C. C., Chen, X., and Dutton, L. (1999) *Nature* **402,** 47–52
50. Sakai, M., and Takahashi, H. (1996) *J. Mol. Struct.* **379,** 9–18
51. Schreiner, S., Steiner, U., and Kramer, H. E. A. (1975) *Photochem. Photobiol.* **21,** 81–84
52. Schreiner, S., and Kramer, H. E. A. (1976) in *Flavins and Flavoproteins* (Singer, T. P., ed) pp. 793–799, Elsevier Science Publishers B. V., Amsterdam
53. McLauchlan, K. A., and Steiner, U. E. (1991) *Mol. Phys.* **73,** 241–263
54. Batchelor, S. N., Kay, C. W. M., McLauchlan, K. A., and Yeung, M. T. (1993) *J. Phys. Chem.* **97,** 4570–4572
55. Song, P.-S. (1968) *Photochem. Photobiol.* **7,** 311–313
56. Medina, M., Vrielink, A., and Cammack, R. (1994) *Eur. J. Biochem.* **222,** 941–947
57. Park, H.-W., Kim, S.-T., Sancar, A., and Deisenhofer, J. (1995) *Science* **268,** 1866–1872
58. Kurreck, H., Bock, M., Bretz, N., Elsner, M., Kraus, H., Lubitz, W., Müller, F., Geissler, J., and Kroneck, P. M. H. (1984) *J. Am. Chem. Soc.* **106,** 737–746
59. Weber, S., Richter, G., Schleicher, E., Bacher, A., Möbius, K., and Kay, C. W. M. (2001) *Biophys. J.* **81,** 1195–1204
60. Zamenhof, P. J., and Villarejo, M. (1972) *J. Bacteriol.* **110,** 171–178
61. Bullock, W. O., Fernandez, J. M., and Short, J. M. (1987) *Biotechniques* **5,** 376–378
62. Stüber, D., Matile, H., and Garotta, G. (1990) *Immunol. Meth.* **4,** 121–152
63. Stoeckelhuber, M., Noegel, A. A., Eckerskorn, C., Köhler, J., Rieger, D., and Schleicher, M. (1996) *J. Cell Sci.* **109,** 1825–1835